Finite Element Analysis
of
Shadow Mask Assembly to
Predict Beam Landing Shift

by

Rajiv Sharma

DPARTMENT OF MECHANICAL ENGINEERING
INDIAN INSTITUTE OF TECHNOLOGY KANPUR

MARCH, 2003

Finite Element Analysis
of
Shadow Mask Assembly to
Predict Beam Landing Shift

A Thesis Submitted
In Partial Fulfillment of the Requirements
for the Degree of
Master of Technology

by

Rajiv Sharma

to the

DPARTMENT OF MECHANICAL ENGINEERING
INDIAN INSTITUTE OF TECHNOLOGY KANPUR

MARCH, 2003

CERTIFICATE

It is certified that the work contained in the thesis entitled **"Finite Element Analysis of Shadow Mask Assembly to predict Beam Landing Shift"**, by **Rajiv Sharma** has been carried out under my supervision and that this work has not been submitted elsewhere for a degree.

Dr. P. M. Dixit
Professor
Department of Mechanical Engg
Indian Institute of Technology Kanpur

March, 2003.

Acknowledgement

I wish to place on records my deep sense of gratitude and indebtedness to my supervisor Dr. P. M. Dixit for his expert guidance, valuable suggestions, personal encouragement and generous help during the course of my thesis. I personally feel that he has inculcated a sense of sincerity and punctuality in me, that shall form a foundation for my future life. His company not only enriched my knowledge but also widened my ways of thinking. From the core of my heart, I thank almighty to have given me an opportunity to work with him.

I am thankful to my colleagues Sachin, Santosh and Amit Pawar of Finite Element Analysis Lab for their constant help and encouragement. I have so many unforgettable memories with them which I'll cherish forever.

But for the constant encouragement of my friends I would not have completed this work. I thank all my friends for always being with me and bearing me through thick and thin. Special thanks to Manisha, Vivek, Saurabh, Manas, Rajat, Gulshan, Vinay, Amar and others whose company at the end of day acted as a relaxant.

Rajiv Sharma

Dedicated to My Parents and Lord Shiva

Abstract

In the present work, thermo-elastic deformation analysis for the shadow mask assembly is performed using NASTRAN to predict beam landing shift due to the thermal deformation of the mask frame assembly.

Since there exists numerous slit type apertures on the shadow mask, it is almost impossible to model the mask as it is. So, the shadow mask is modeled and analyzed as a thin plate with no apertures, introducing effective thermal conductivity and effective elastic constants. The effective properties are determined by subjecting a typical element to suitable boundary conditions and measuring appropriate quantities. The heat transfer in shadow mask is treated as a 2-D problem and formulation for the thermal analysis of a flat plate is used. The formulation for the plate bending analysis is used to calculate the thermal deformation of the mask under temperature induced strains and displacement boundary conditions. The three noded flat plate triangular element is employed for the analysis. Two test problems are solved to validate the formulation for 2-D thermal analysis and plate bending analysis of flat plate.

The beam landing shift of the present work (using NASTRAN) is compared with the results from published literature. It is observed that the temperature of shadow mask first increases and then stabilizes to a particular value. The beam landing shift on the panel first increases and then decreases to settle to a lower value.

Contents

List of Figures

List of Tables

List of symbols

A_{mask}	Area of shadow mask.
A_s	Area of aperture.
[B]	Matrix relating the linear strain to the nodal displacement.
c	Specific heat.
C_{ij}	Component of capacitance matrix.
$[C]$	Capacitance matrix.
D_{ijkl}	Elastic stiffness tensor.
$[D]$	Elastic stiffness matrix.
e_h	Horizontal retrace time/time for scanning one line.
e_v	Vertical retrace time/time for scanning the whole screen.
E	Youngs modulus.
E_x, E_y	Effective Youngs modulus in x and y directions, respectively.
F_x, F_y	Total reaction in x and y direction.
$\{F\}$	Global thermal force vector.
$[F]$	Global force vector.
$[J]$	Jacobian matrix.
k_x, k_y	Effective thermal conductivities in x and y directions, respectively.
$[K]$	Stiffness matrix.
N_i, N_j	Shape function.
$[N]$	Shape function matrix.
P	Power of electron beam.
PH	Horizontal pitch of the shadow mask.
PV	Vertical pitch of the shadow mask.

$q_{in(mask)}$ Heat input into the mask.

q_{out} Radiation heat flux out of the shadow mask into the surroundings.

Q_i Global heat flux vector.

$\dot{Q}$ Heat generation per unit area of mask.

t Thickness of shadow mask.

$\bar{t}_x, \bar{t}_y, \bar{t}_z$ Specified tractions in the x, y and z directions respectively.

T_j Temperature at node j.

T Temperature at a point.

T_{s1}, T_{s2}, T_s Surface temperatures.

T_0 Initial temperature.

ΔT Increment in temperature.

$\{T\}$ Temperature vector.

$u_0(x, y)$ x displacement at the middle surface of the plate.

$v_0(x, y)$ y displacement at the middle surface of the plate.

$\hat{u}$ Specified displacement on boundaries.

w_i weight.

W_i Internal work done.

W_e External work done.

$\Delta\tau$ Time increment.

$\varepsilon_1, \varepsilon_2$ Emmisivities of the front and rear surface of shadow mask.

ε_0 Initial thermal strain.

ε_{kl} strain tensor developed in the body.

$\{\varepsilon\}$ Matrix representation of strain tensor.

δ_{kl} Kronecker's delta.

λ, μ	Lame's constants.
υ	Poisson's ratio.
ρ	Density.
σ_{ij}	Cauchy stress tensor.
$[\sigma]$	Matrix representation of Cauchy stress tensor.
ξ, η, ζ	Natural coordinate.

Chapter 1
Introduction

1.1. Introduction

A shadow mask is a thin membrane structure with numerous apertures, and is located behind a panel or a C.R.T. screen, so that the electron beams transiting through the apertures can strike the phosphors spread on the back of the screen. The thermal expansion of the mask frame assembly due to electron bombardment during operation causes a change in relative distance between the shadow mask and the phosphors. This results in a landing shift on the phosphor screen and, consequently deteriorates color purity. Predicting the temperature rise and beam landing shift is one of the most common requirement for designing the shadow mask type cathode ray tube (CRT). With increasing demands for a large size of C.R.T. with high resolution, the decolorization due to thermal deformation of a shadow mask has been an important subject of study.

1.2. Review of literature

Analysis of thermal deformation in a shadow mask and calculation of the corresponding landing shift of electron beams on the screen helps in improving the design of a shadow mask. A number of attempts have been made to suppress the thermal landing shift or mislanding on the screen. Since the development of the shadow mask for the color television tube [1], rimmed steel or Al-killed steel has been mainly used as its material. Inaba *et al* [1] proposed lowering the thermal expansion of the mask and enhancing the thermal radiation of the mask. Invar (Fe-36Ni) shadow mask was developed with its thermal expansion coefficient about one-tenth of the conventional mask. But even the Invar shadow mask CRT has a landing shift of the order of a few micrometer and needs to be designed precisely.

The temperature of the mask during operation is measured by a thermocouple and it is assumed that the temperature of the mask is uniform over its area. Kim *et al* [2] proposed a non-contact method of measuring the temperature distribution of the shadow mask during operation by the radiation thermometer using an InSb photo-sensor to predict the correct temperature distribution in the shadow mask.

Since the advent of shadow mask for CRT's, bimetal springs were used to compensate for mask doming [3]. The bimetal system, operated by bending characteristics of bimetals attached to support spring, moves the shadow mask assembly towards the screen in such a way that the apertures follow the electron beam path. A corner-support system has been developed [4] that sets pins at an angle to the panel side wall so as to make the angle between the electron-beam path and the fiat-plate spring approximately equal to 90°. However, it necessitates the manufacturer to use a complex support mechanism to avoid disengagement of the spring and the pin under mechanical loads. To compensate for the thermal mislanding [5], self-thermal compensator (STC), a component of the shadow mask assembly is attached to the frame. Still, it is difficult to control the compensation of the thermal mislanding for high resolution CRTs.

Kim and Im [3] performed the finite element analysis for calculating the landing shift. They calculated the effective thermal conductivity and effective elastic modulus and developed a simplified model for estimating the surrounding temperatures. Okada and Ikegaki [6] simulated the landing shift by structural analysis using finite element method and measured data of temperature and showed that thermal deformation was effectively suppressed when the shape of shadow mask surface had comparatively large curvature on the horizontal axis and small curvature on the diagonal axis.

One of the disadvantages of the above researches, however, is that these analysis procedures require measured data of shadow mask. Kim and Kim [7] analyzed the transient thermo-elastic deformation by FEM using the ANSYS computer program and calculated the beam landing shift by considering all parts inside the tube. Park *et*

al [5] simulated the landing shift by using the finite element method (FEM) employing ANSYS, thus allowing the elimination of prototyping and making the search for an optimal design of the shadow mask more efficient.

In the above analysis, the shadow mask is modeled as a thin plate without slits but using the effective material properties [3]. A thin plate simultaneously supports membrane and bending actions. In classical thin plate theory, transverse shear deformation is neglected. However, most finite element formulation for plates and shells employ the first-order plate theory which accounts for the transverse shear deformation. When the plate is sufficiently thin and the loads are smoothly distributed, Reissner theory [8] is sufficiently accurate for the determination of stress and displacement.

1.3. Objective of the present work

The objective of the present work is to analyze the transient thermo-elastic deformation of the shadow mask assembly using the finite element method (FEM) through the NASTRAN computer program and calculate the beam landing shift on the screen. For this purpose, the shadow mask is treated as a thin plate with effective material properties. First, two-dimensional thermal analysis is done to determine the temperature distribution. After analyzing the temperature distribution, we perform the thermo-elastic deformation analysis using the plate bending theory. Finally, the landing shift of the electron beams is predicted.

1.4. Structure of the thesis

Chapter 2 deals with brief description of shadow mask, together with its support system, which compensates for the landing shifts of electron beams. The governing equation for heat transfer involving in-plane conduction and out of plane radiation is formulated and the finite element formulation is described including the nature of finite elements employed. Chapter 3 deals with the formulation of the transient thermal deformation of the mask frame assembly under temperature induced thermal

strains using the plate bending theory. The fourth chapter consists of the validation problems. The beam landing shift is predicted in the fifth chapter. The last chapter summarizes the work carried out and suggests the possible further scope of the present work.

Chapter 2

Thermal Analysis

2.1 Description of the shadow mask

The shadow mask is used as a barrier to separate the individual color selecting electron beams, which are designed to strike the color phosphors [2]. Because the three electron beams, red, green and blue arrive at slightly different angles (from the three separate electron guns), see Fig. 2.1, it is possible to construct and align the shadow mask such that the electron beam from one gun will strike the correct phosphor dot, but the other two phosphors will be in shadow. This way, the intensity of red, green and blue can be separately controlled at each dot triad location.

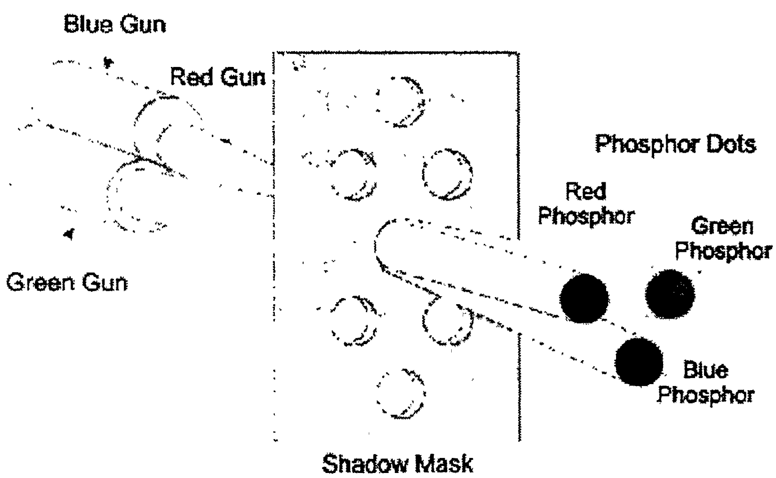

Fig. 2.1 Working of shadow mask

The shadow mask assembly consists of a shadow mask with numerous apertures, frame, and support springs. The shadow mask has a great number of apertures, the size and shape of which vary with thickness in order to prevent dispersion of electron beams. The three beams are projected onto their preselected phosphors through an aperture in the shadow mask. The geometry of the mask is expressed by the two-step curvature and the aperture shape is of slit type. Because the geometry is expressed by

two-step curvature, Bezier surface is relied upon to express the geometry of the mask. The Bezier surface represents a curved surface via best approximation from vertex coordinates in the rectangular region, and this yields almost exact representation for surface with small curvatures such as shadow mask. The equation of the Bezier surface [9] is given as,

$$f(x,y)=\sum_{i=1}^{m}\sum_{j=1}^{n} f(x_i,y_j)J_{n-1,j-1}(u)J_{m-1,i-1}(w) \tag{2.1a}$$

where, $f(x_i,y_j)$ are the vertices of the characteristic polyhedron that form an $(m+1)\times(n+1)$ rectangular array of points, and

$J_{n,i}$ is Bernstein polynomial given as,

$$J_{n,i}=\binom{n}{i}u^i(1-u)^{n-i}\ ;\ 0\le u,w\le 1 \tag{2.1b}$$

The shadow mask and surrounding frame are connected by spot welding at several points and the support springs are attached to the edge or to the corners of the frame. The shadow mask assembly is supported by the support springs fitted into the tapered stud on the C.R.T. wall. There are two types of shadow masks, when classified according to the way a shadow mask is connected to the frame surrounding the shadow mask:

1) Bimetal system : It operates by bending characteristics of bimetals attached to the support spring.
2) Corner suspension: Direct compensation system, which depends solely on the geometry of the support spring.

Both of these springs are designed to compensate for the landing shift of a beam resulting from thermal deformation by moving the shadow mask assembly towards the screen in such a way that the apertures follow the electron beam path.(see Fig 2.2)

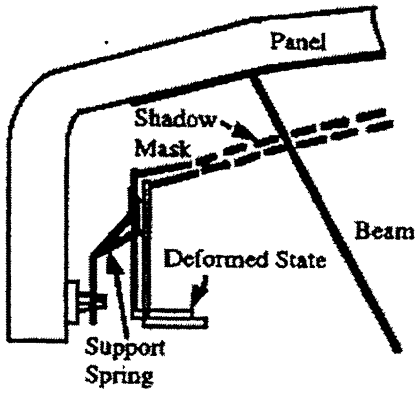

Fig. 2.2 Compensation of beam mislanding by the support spring

A magnetic shield is attached to the bottom of the frame to prevent the change of beam trajectory due to the magnetization from the environmental magnetic field and to prevent the degradation of picture by stray electrons. The entire interior of CRT is coated with conductive coatings. The inside of the C.R.T. is in a high vacuum state for the electron beams to travel without being disturbed by air. Since high voltage difference exists between the shadow mask and electron guns, a large percentage of the beam energy is converted into heat energy and a little portion of beam is reflected. Transmitted beams through the apertures in the shadow mask do not directly contribute to temperature rise. The heat in the shadow mask is transferred via heat conduction in the in-plane directions and via heat radiation on the surface. Heat radiation is the more dominant heat transfer mechanism than heat conduction and the major parts of the heat energy ultimately flow out through radiation. The heat radiating into the inner walls of the C.R.T. from the surface of the shadow mask raises the surrounding temperature.

2.2 Analysis procedure

To predict beam-landing shift quantitatively, we must perform four analysis steps in sequence [7]:

1. Effective material properties in the effective area of the shadow mask are calculated from thermal conductivity and elastic modulus in the shadow mask material and from the shape and layout of the apertures in the shadow mask

2. Transient temperature distributions of all parts inside the tube are calculated with the consideration of the heat radiation and the heat conduction between each part.
3. The transient thermal deformation of the mask frame assembly is obtained from the temperature distribution.
4. The beam landing shift on the phosphor screen is calculated from the relative distance between the panel and the shadow mask, the thermal deformation of the shadow mask and the position of the beam's deflection center.

These four steps are illustrated in Fig. 2.3

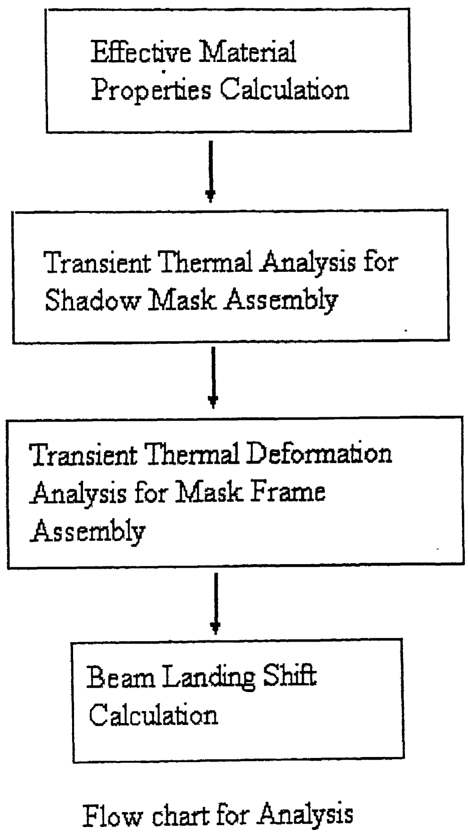

Fig. 2.3 Flow chart for analysis procedure

2.3 Assumptions

1. The line velocity of the electron beam with respect to the surface of the shadow mask is assumed to be constant regardless of position and time.
2. The motion of electron beam is straight started from a fixed deflection center.

3. The heat input per unit area in the shadow mask can be obtained by taking into account the size of the aperture observed from the electron gun side and the retrace time (time during which the electron beams are not emitted from the electron guns) as well as the power from the electron gun.

$$q_{in(mask)} = \frac{P}{A_{mask}}(1-e_h)(1-e_v)(1-\frac{A_s}{PH * PV}) \tag{2.2}$$

where,

P : Power of electron beam,

A_{mask} : Total area of shadow mask,

A_s : Area of aperture,

e_h : horizontal retrace time/time for scanning one line,

e_v : vertical retrace time/time for scanning the whole screen.

PH : Horizontal pitch of the shadow mask.

PV : Vertical pitch of the shadow mask.

4. Since it is too complicated to consider all geometry inside the C.R.T. system, an simplified axisymmetric model as shown in Fig. 2.4 is considered [3]. We then replace this simplified model with an equivalent model with surrounding temperatures and the associated emissivities. This is also shown in Fig. 2.4. The

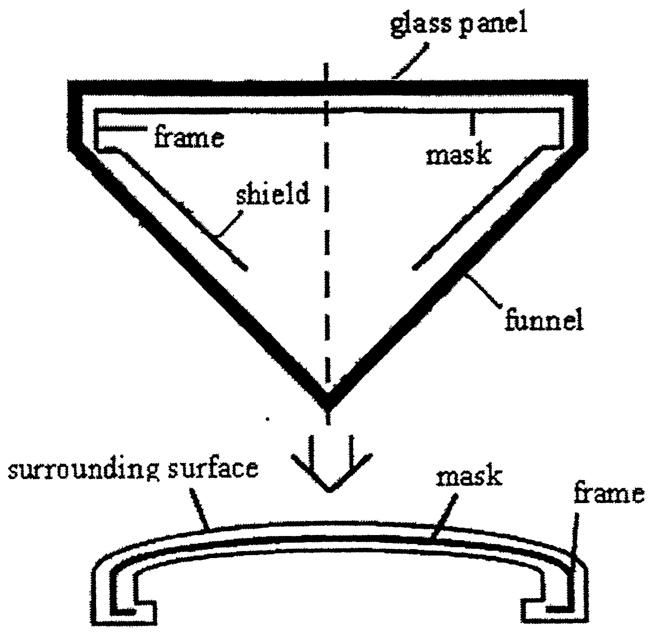

Fig. 2.4 Axisymmetric model for mask-frame assembly

equivalent emissivities and equivalent temperatures for the surrounding surface are determined such that the heat flux between the mask and the surroundings be equivalent to the heat flux in the original model. The radiation heat flux out of the shadow mask into the surroundings is then written as,

$$q_{out} = \varepsilon_1 \sigma (T^4 - T_{s1}^4) + \varepsilon_2 \sigma (T^4 - T_{s2}^4) \qquad (2.3)$$

where,

T : temperature (°K) of the shadow mask,

$\varepsilon_1, \varepsilon_2$: emissivities of the front and the rear surfaces respectively,

T_{s1}, T_{s2} : surrounding temperatures(°K) of the front and the rear surfaces, respectively,

σ : Stefan-Boltzmann constant (5.669 x10^{-8} W/m^{2}K^4).

5. Since there exist numerous slit type apertures on the shadow mask, it is almost impossible to model the shadow mask as it is. Therefore we replace the shadow mask by a thin plate of the same size with no apertures, introducing so called the effective thermal conductivity and effective elastic constants [3].The effective properties are determined by subjecting a typical element (shown in Fig. 2.5) to suitable boundary conditions and measuring appropriate quantities.

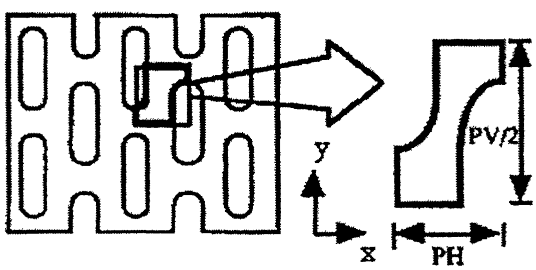

Fig. 2.5 Model for effective material constants

a. Effective Thermal Conductivity (k_x and k_y) [10]: To evaluate the effective thermal conductivity in the x-direction, we impose a constant temperature on the right side and prescribe a heat flux on the left side while the top and bottom side are insulated. Fig. 2.6 shows these boundary conditions for evaluation of k_x. Similar boundary conditions are applied for the evaluation of k_y also (see Fig. 2.6).

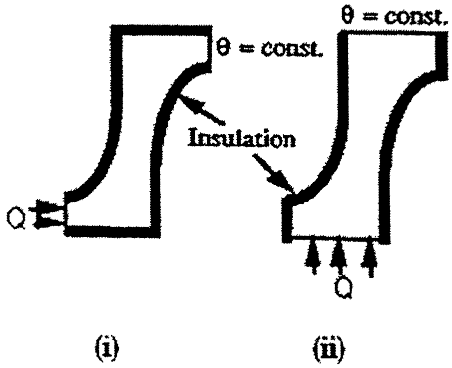

Fig. 2.6 Boundary conditions for evaluation of thermal conductivities

Thus we have in x-direction,

$$-k_x = \frac{2Q}{PV}\frac{PH}{\Delta T} \tag{2.4}$$

Similarly, we can have in the y-direction,

$$-k_y = \frac{Q}{PH}\frac{PV}{2\Delta T} \tag{2.5}$$

b. Effective Elastic constants (E_x, υ_x, E_y, υ_y) [10] : For determining the effective elastic constants in x direction, the lower and left sides are simply supported. Further a uniform displacement in x-direction is imposed on the right side while the constraint of the uniform displacement in the y direction is maintained upon the top side, (See Fig. 2.7).Young's modulus and Poisson's ratio in the x-direction are then given as,

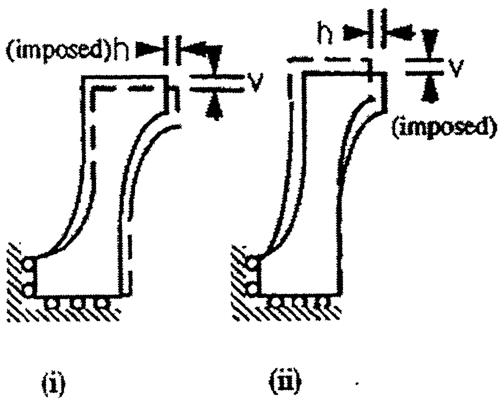

Fig. 2.7 Boundary conditions for evaluation of effective elastic moduli

$$E_x = (\frac{2F_x}{PV})(\frac{PH}{h}) \qquad (2.6a)$$

$$\upsilon_{xy} = (\frac{2v}{PV})(\frac{PH}{h}) \qquad (2.6b)$$

where F_x if the total reaction force in the x direction on the right side. Effective properties in the y direction can be found similarly as,

$$E_y = (\frac{F_y}{PH})(\frac{PV}{2v}) \qquad (2.7a)$$

$$\upsilon_{yx} = (\frac{h}{PH})(\frac{PV}{2v}) \qquad (2.7b)$$

6. The curvature of the shadow mask is assumed small. Therefore, it can be approximated as a plate.
7. The initial temperature of the shadow mask assembly (T_o) is taken to be 25 °C.

2.4 Governing equation and boundary and initial conditions

Electron beams emitted from electron gun collide with the Shadow Mask and generate heat energy and the heat is transferred to other parts via heat conduction and heat radiation. Thermal analysis of Shadow Mask is done to obtain transient temperature distribution of shadow mask assembly which is utilized to obtain deformation due to thermal forces in the shadow mask assembly and eventually predict beam landing shift.

Since the thickness of the shadow mask is very small, the temperature gradient and heat flux in the thickness direction are almost negligible. Thus, the problem of heat transfer in the shadow mask can be considered as a 2-D problem where the incident heat flux and the radiation losses are included in the heat generation term.

Consider an elementary area dA ($dA = dx \times dy$) as shown in Fig. 2.8. Let, $\dot{Q}$ be the heat generation/unit area and, k_x , k_y be the thermal conductivities in x and y

direction respectively . Further, ρ and c be the density and specific heat respectively.

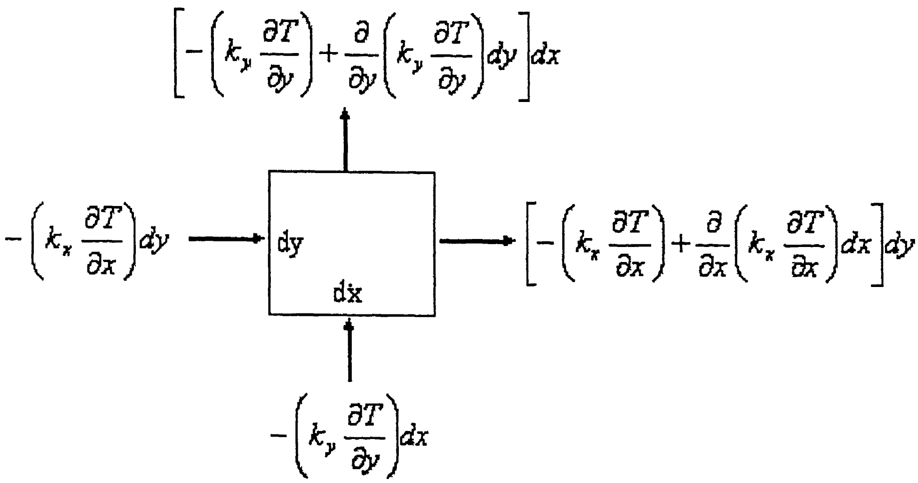

Fig. 2.8 Heat exchange between faces

Then the heat balance equation becomes,

$$\frac{\partial}{\partial x}(k_x\frac{\partial T}{\partial x})+\frac{\partial}{\partial y}(k_y\frac{\partial T}{\partial y})+\dot{Q}-\rho c\frac{\partial T}{\partial \tau}=0 \tag{2.8}$$

where, τ denotes the time. The, heat generation term includes the heat input into the bottom surface of the mask (through the electron beams) and the heat radiating out of the surface to the surrounding. Thus we have,

$$\dot{Q}=\{q_{in}-[\varepsilon_1\sigma(T^4-T_{s1}^4)+\varepsilon_2\sigma(T^4-T_{s2}^4)]\} \tag{2.9}$$

Since, the surrounding temperature is same for both the surfaces and the emmisivities of the two surfaces are also the same,

$$\left.\begin{aligned}\varepsilon_1=\varepsilon_2=\varepsilon\\ T_{s1}=T_{s2}=T_s\end{aligned}\right\} \tag{2.10}$$

The equation (2.9) becomes,

$$\dot{Q}=q_{in}-[2\varepsilon\ \sigma(T^4-T_s^4)] \tag{2.11}$$

Then the governing equation (2.8) becomes,

$$\frac{\partial}{\partial x}(k_x\frac{\partial T}{\partial x})+\frac{\partial}{\partial y}(k_y\frac{\partial T}{\partial y})+q_{in}-[2\varepsilon\ \sigma(T^4-T_s^4)]-\rho c\frac{\partial T}{\partial \tau}=0 \tag{2.12}$$

The boundary condition of the problem is,

$$-k\frac{\partial T}{\partial n}=0 \qquad \text{on } \Gamma \qquad (2.13)$$

where, Γ is the boundary of the shadow mask which is assumed to be insulated. The initial condition of the problem is,

$$T=T_0 \qquad \text{at } \tau=0 \qquad (2.14)$$

2.5 Finite element formulation

The domain is discretised into n_e number of elements. Over a typical element e, the temperature is approximated as,

$$T=\sum_{j=1}^{n_n} N_j(x,y)T_j^e(\tau) \qquad (2.15)$$

where, n_n is the number of nodes per element, $T_j^e(\tau)$ is the time-dependent (unknown) nodal temperature at the local node j of the element and $N_j(x,y)$ is the (known) shape function corresponding to node j. The expression (2.15) can be considered an approximate solution of the problem consisting of the differential equation (2.12) and boundary condition (2.13) if the following weighted integral is zero,

$$\int_{A^e} w_i\left[\frac{\partial}{\partial x}\left(k_x\frac{\partial T}{\partial x}\right)+\frac{\partial}{\partial y}\left(k_y\frac{\partial T}{\partial y}\right)\right]dA+\int_{A^e} w_i q_{in}\,dA-2\int_{A^e} w_i\varepsilon\sigma(T^4-T_s^4)\,dA-\int_{A^e} w_i\rho c\frac{\partial T}{\partial \tau}dA=0 \qquad (2.16)$$

Here, A^e is the area of typical element and w_i is the weighting function. Using Green's lemma and the boundary condition (2.13), the first integral can be simplified. When it is simplified, equation (2.16) becomes,

$$\int_{A^e}\left(\frac{\partial w_i}{\partial x}k_x\frac{\partial T}{\partial x}+\frac{\partial w_i}{\partial y}k_y\frac{\partial T}{\partial y}\right)dA-\int_{A^e} w_i q_{in}\,dA+2\int_{A^e} w_i\varepsilon\sigma(T^4-T_s^4)\,dA+\int_{A^e} w_i\rho c\frac{\partial T}{\partial \tau}dA=0 \qquad (2.17)$$

For Galerkin's formulation, weighting functions are given by

$$w_i=N_i \qquad (2.18)$$

Substituting equations (2.15) and (2.18) into expression (2.17), we get,

$$\sum_{j=1}^{n_n} C_{ij}^e \frac{\partial T_j^e}{\partial \tau} + \sum_{j=1}^{n_n} K_{ij}^e T_j^e = Q_i^e \tag{2.19}$$

where,

$$C_{ij}^e = \int_{A^e} \rho c N_i N_j dA \text{ , Element capacitance matrix,} \tag{2.20}$$

$$K_{ij}^e = \int_{A_e} \left(\frac{\partial N_i}{\partial x} k_x \frac{\partial N_j}{\partial x} + \frac{\partial N_i}{\partial y} k_y \frac{\partial N_j}{\partial y} \right) dA + 2 \int_{A_e} \varepsilon \sigma T^3 N_i N_j dA \text{ ,} \tag{2.21}$$

Element conductivity matrix

$$Q_i^e = \int_{A_e} q_{in} N_i dA + 2 \int_{A_e} \varepsilon \sigma T_s^4 N_i dA. \text{ , Element heat flux vector} \tag{2.22}$$

Note that, while arriving at equation (2.19) the term T^4 has been approximated as

$$T^4 = T^3 \left(\sum_{j=1}^{n_n} N_j T_j^e \right) \tag{2.23}$$

As a result, the matrix K_{ij} contains T^3 term where T is unknown. Thus equation (2.19) becomes a nonlinear equation, which has to be solved by iteration.

Assembling the elemental equation (2.19) over all the elements, the global equation becomes,

$$\sum_{j=1}^{n} C_{ij} \frac{\partial T_j}{\partial \tau} + \sum_{j=1}^{n} K_{ij} T_j = Q_i \tag{2.24}$$

where n is the number of total nodes of the domain, C_{ij} is the global capacitance matrix, K_{ij} is the global conductivity matrix, Q_i is the global heat flux vector and T_j represents the (unknown) temperature at global node j.

Equation (2.24) is a system of ordinary differential equations. To convert it into a set of algebraic equations, a direct time integration technique like the forward difference scheme is used .For this purpose ,the time axis is divided into various time steps using discrete time values τ^k, k = 0,1,2......... Let the values of nodal

temperatures T_j at times τ^k and τ^{k+1} be T_j^k and T_j^{k+1} respectively .Then according to the finite difference scheme,

$$\frac{\partial T_j^k}{\partial \tau} = \frac{T_j^{k+1} - T_j^k}{\Delta \tau} \tag{2.25}$$

Writing equation (2.24) at time τ^k and eliminating $\left(\frac{\partial T_j^k}{\partial \tau}\right)$ using (2.25) ,we get the following set of algebraic equations,

$$\sum_{j=1}^{n} C_{ij} T_j^{k+1} = F_j^k \tag{2.26}$$

where, $$F_j^k = \sum_{j=1}^{n} (C_{ij} - \Delta\tau K_{ij}) T_j^k + \Delta\tau Q_j^k . \tag{2.27}$$

This set of equation is in index form. Writing the above equation in matrix form, we have

$$[C]\{T\}^{k+1} = \{F\}^k \tag{2.28}$$

The set of equation (2.28) is solved sequentially for the discrete times τ^1, τ^2,...etc. For the first time step, the right side vector is evaluated using the initial condition

$$T_j^0 = T_o \tag{2.29}$$

2.6 Numerical integrations

The terms of the capacitance matrix $[C]$ and vector $\{F\}$ involve surface integrals which are difficult to evaluate analytically. Therefore numerical integration has to be applied to obtain the solution. The integrals (2.20) – (2.22) are evaluated using Gauss quadrature. In the present work, three-noded triangular element is used. Since the Gauss numerical integration formula is available only for the standard triangle, first the element is transformed into the standard triangle using the natural coordinates (see Fig 2.9). The transformation is given by,

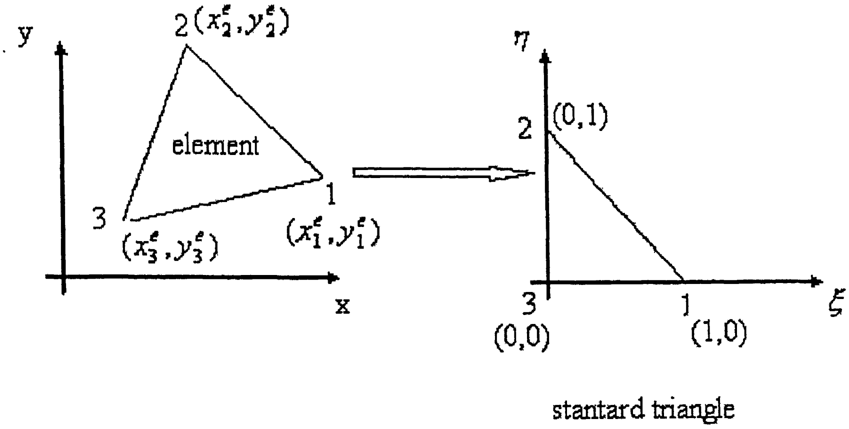

Fig 2.9 Coordinate Transformation

$$\left.\begin{aligned} x &= \alpha_1 + \alpha_2 \xi + \alpha_3 \eta \\ y &= \beta_1 + \beta_2 \xi + \beta_3 \eta \end{aligned}\right\} \tag{2.30}$$

where, the constants α_i and β_i are determined from the conditions that the three vertices of the element get mapped onto the three vertices of the standard triangle. The Jacobian matrix for the transformation is given as,

$$[J] = \begin{bmatrix} \frac{\partial x}{\partial \xi} & \frac{\partial x}{\partial \eta} \\ \frac{\partial y}{\partial \xi} & \frac{\partial y}{\partial \eta} \end{bmatrix} \tag{2.31}$$

The Jacobian matrix is evaluated using the transformation (2.30) .Then the integral (2.20) gets transformed as

$$C_{ij}^e = \int_0^1 \int_0^{1-\xi} \rho c N_i N_j \det[J] d\xi d\eta \tag{2.32}$$

Then, applying the Gauss numerical integration formula [11], we get

$$C_{ij}^e = \sum_{r=1}^{n_G} \frac{1}{2} w_r \left(\rho c N_i N_j \det[J]\right)\Big|_{(\xi_r, \eta_r)} \tag{2.33}$$

where n_G is the number of Gauss points, (ξ_r, η_r) are the (natural) coordinates of the gauss points and w_r are the corresponding weights. The integrals (2.21) and (2.22) are evaluated similarly:

$$K_{ij} = \sum_{r=1}^{n_G} \frac{1}{2} w_r \left\{ \left(\frac{\partial N_i}{\partial x} k_x \frac{\partial N_j}{\partial x} + \frac{\partial N_i}{\partial y} k_y \frac{\partial N_j}{\partial y} \right) + 2\varepsilon\sigma T^3 N_i N_j \right\} \det[J] \Bigg|_{(\xi_r, \eta_r)} \tag{2.34}$$

$$Q_i = \sum_{r=1}^{n_G} \frac{1}{2} w_r \left(q_{in} N_i + 2\varepsilon\sigma T_s^4 N_i \right) \det[J] \Big|_{(\xi_r, \eta_r)} \tag{2.35}$$

The elements of the matrix are numerically integrated using three integration points located at the element midpoints of the three sides.

Chapter 3

Deformation Analysis

3.1 Introduction

The second step in the analysis procedure is to calculate the transient thermal deformation of the mask frame assembly under temperature induced thermal strains and displacement boundary conditions. This is done by idealizing the shadow mask as a thin plate and using the governing equations of plate bending theory.

3.2 Plate bending theory

3.2.1 Basic assumptions

Consider a plate with xy plane coinciding with the plate's midplane and the z coordinate perpendicular to it and directed downwards. The fundamental assumptions are as follows [12]:

1. It is assumed that the lines of material points, which are straight and normal to the undeformed middle surface of the element, remain straight but not necessarily normal to the middle surface after deformation.
2. The strain energy corresponding to stresses perpendicular to the middle surface is disregarded, i.e. the stress component normal to the plate mid-surface is constrained to be zero in the constitutive equations.
3. The plate thickness remains constant during the deformation.

Assumption (1) is equivalent to taking into account the effect of transverse shear deformation and it has been widely used in the context of linear and nonlinear analysis of thin plates. On the other hand, assumption (2) is similar to one of the plane stress conditions. Finally, assumption (3) implies that the thickness of the plate at

each point does not change in different deformed configurations of the plate, which implies zero strain along the thickness direction.

The deformation is governed by the following three sets of governing equations :

1. Stain-displacement equations.
2. Equilibrium equations.
3. Constitutive equations.

3.2.2 Strain-displacement equations

Assumptions (1) and (3) imply that the displacement components (u, v, w) of any arbitrary point (x, y, z) in the plate can be expressed as [13]:

$$\left.\begin{aligned} u &= u_0(x,y) + z\phi_x(x,y) \\ v &= v_0(x,y) + z\phi_y(x,y) \\ w &= w(x,y) \end{aligned}\right\} \tag{3.1}$$

where $u_0(x,y)$ and $v_0(x,y)$ are the displacements of the middle surface of the plate. Further, ϕ_x and ϕ_y are the rotation angles of the lines normal to the undeformed neutral surface in the x-z and y-z plane, respectively.

The five significant strain components may be expressed as:

$$\varepsilon_{xx} = \frac{\partial u}{\partial x} \tag{3.2a}$$

$$\varepsilon_{yy} = \frac{\partial v}{\partial y} \tag{3.2b}$$

$$\varepsilon_{xy} = \frac{1}{2}\left(\frac{\partial u}{\partial y} + \frac{\partial v}{\partial x}\right) \tag{3.2c}$$

$$\varepsilon_{yz} = \frac{1}{2}\left(\frac{\partial v}{\partial z} + \frac{\partial w}{\partial y}\right) \tag{3.2d}$$

$$\varepsilon_{zx} = \frac{1}{2}\left(\frac{\partial u}{\partial z} + \frac{\partial w}{\partial x}\right) \tag{3.2e}$$

3.2.3 Equilibrium equations

It is assumed that the body and inertial forces are negligible. Therefore, the stress components must satisfy the following differential equation of equilibrium, such that the divergence of the stress tensor must vanish. Thus,

$$\sigma_{ij,j} = 0 \tag{3.3}$$

3.2.4 Constitutive equations

The constitutive equation used is the generalized Hooke's law relating the stress and strain components.

$$\sigma_{ij} = D_{ijkl}\left(\varepsilon_{kl} - \varepsilon_{0kl}\right) \tag{3.4}$$

where,

ε_{kl} : is the strain developed in the body.

ε_{0kl} : is the initial strain developed due to differential heating.

D_{ijkl} : Constitutive tensor.

The expression for the constitutive tensor for isotropic material is,

$$D_{ijkl} = \lambda\delta_{ij}\delta_{kl} + 2\mu\delta_{ik}\delta_{jl} \tag{3.5}$$

where, λ and μ are Lame's constants. The expression for the initial strain ε_{0kl} is,

$$\varepsilon_{okl} = \alpha\Delta T\delta_{kl} \tag{3.6}$$

where,

α : Coefficient of thermal expansion.

ΔT : Temperature rise.

δ_{kl} : Kronecker's delta.

3.2.5 Boundary conditions

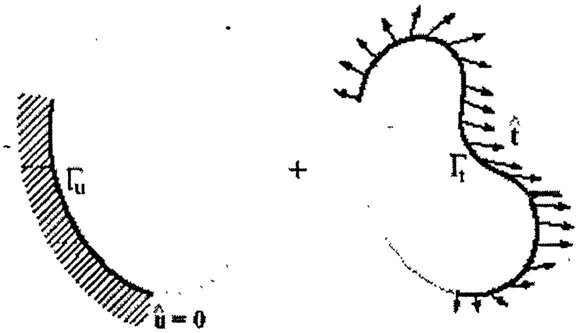

Fig. 3.1. Boundary conditions

There are two types of boundary conditions, which may be stated as:

1. Displacement boundary condition: Displacement is prescribed on the boundary. Thus,

$$\left.\begin{aligned} u &= \hat{u} \\ v &= \hat{v} \\ w &= \hat{w} \end{aligned}\right\} \quad \text{on } \Gamma_u \qquad (3.7)$$

   where Γ_u is the boundary on which displacements are specified, and $(\hat{u}, \hat{v}, \hat{w})$ represents the specified displacement on the boundary.

2. Traction boundary condition: Traction is prescribed on the boundary. Thus,

$$\left.\begin{aligned} \sigma_{xx} n_x + \sigma_{xy} n_y + \sigma_{xz} n_z &= \bar{t}_x \\ \sigma_{xy} n_x + \sigma_{yy} n_y + \sigma_{yz} n_z &= \bar{t}_y \\ \sigma_{xz} n_x + \sigma_{yz} n_y + \sigma_{zz} n_z &= \bar{t}_z \end{aligned}\right\} \text{ on } \Gamma_t \qquad (3.8)$$

   where Γ_t is the boundary on which tractions are specified, (n_x, n_y, n_z) are the components of unit outward normal to Γ_t and $(\bar{t}_x, \bar{t}_y, \bar{t}_z)$ represent the specified tractions in the x, y and z directions respectively.

3.2.6 Variational formulation

The principle of virtual work can be stated as, "If the displacements corresponding to the exact solution to the problem are perturbed by adding arbitrary virtual displacements, then the work done by the external forces along these virtual displacements equals the work done by the stresses along the corresponding virtual strains". Thus, for equilibrium to be ensured, the total potential energy must be stationary for variation of admissible displacements. Thus we can write:

$$\delta\Pi = (\delta W_i - \delta W_e) = 0 \tag{3.9}$$

where,

$\delta\Pi$ is the total potential energy for variation of admissible displacements,

δW_e is the external work done by forces along the virtual displacements,

δW_i is the internal work done by stress along virtual strains.

The external work done along the virtual displacements can be expressed as:

$$\delta W_e = \int_{\Gamma_t} (\bar{t}_x\, \delta u + \bar{t}_y\, \delta v + \bar{t}_z\, \delta w)\, d\Gamma \tag{3.10}$$

where $(\delta u, \delta v, \delta w)$ are the components of virtual displacement. Further, the internal work done is given by:

$$\delta W_i = \int_V \delta\left(\varepsilon_{ij} - \varepsilon_{oij}\right)\sigma_{ij}\, dV \tag{3.11}$$

where, V represents the domain volume, $\delta\varepsilon_{ij}$ is the virtual strain and $\delta\varepsilon_{oij}$ is the virtual initial strain. Thus, the total variation in potential energy becomes:

$$\delta\Pi = \left(\int_V \delta\left(\varepsilon_{ij} - \varepsilon_{oij}\right)\sigma_{ij}\, dV - \int_{\Gamma_t} (\bar{t}_x\, \delta u + \bar{t}_y\, \delta v + \bar{t}_z\, \delta w)\, d\Gamma \right) = 0 \tag{3.12}$$

3.3. Finite element formulation

3.3.1. Matrix notation

Matrix Notation is used in the development of finite element equations. The displacement vector at any point in the domain is defined as:

$$\{u\} = \{u, v, w\}^T \tag{3.13}$$

The components of the strain tensor ε_{ij} are represented in array form as follows:

$$\{\varepsilon\} = \{\varepsilon_{xx}, \varepsilon_{yy}, 2\varepsilon_{xy}, 2\varepsilon_{yz}, 2\varepsilon_{xz}\}^T \tag{3.14}$$

The components of the initial strain tensor ε_{oij} are similarly represented as an array $\{\varepsilon_o\}$. The components of the stress tensor σ_{ij} are represented in array form as follows:

$$\{\sigma\} = \{\sigma_{xx}, \sigma_{yy}, \sigma_{xy}, \sigma_{yz}, \sigma_{zx}\}^T \tag{3.15}$$

Thus, the constitutive relation (3.4) becomes,

$$\{\sigma\} = [D](\{\varepsilon\} - \{\varepsilon_o\}) \tag{3.16}$$

where the components of constitutive matrix $[D]$ for an isotropic material may be written as:

$$[D] = \frac{E}{1-\upsilon^2}\begin{bmatrix} 1 & \upsilon & 0 & 0 & 0 \\ \upsilon & 1 & 0 & 0 & 0 \\ 0 & 0 & \frac{1-\upsilon}{2} & 0 & 0 \\ 0 & 0 & 0 & \frac{1-\upsilon}{2} & 0 \\ 0 & 0 & 0 & 0 & \frac{1-\upsilon}{2} \end{bmatrix} \tag{3.17}$$

here, E is the Young's modulus and υ is poisson's ration.

The expression for total potential energy given by eq. (3.12) can be expressed using the above matrix notations, in the following form:

$$\delta\Pi = \left(\int_V \delta(\{\varepsilon\} - \{\varepsilon_o\})^T [D](\{\varepsilon\} - \{\varepsilon_o\}) dV - \int_{\Gamma_t} \delta\{u\}^T \{\bar{t}\} d\Gamma \right) = 0 \tag{3.18}$$

where, $\{\bar{t}\} = \{\bar{t}_x, \bar{t}_y, \bar{t}_z\}^T$ (3.19)

3.3.2. Flat plate element

The flat plate element is formulated by the combination of a plane stress element and a plate-bending element [12]. Five degrees of freedom are specified at each nodal point, corresponding to three displacements and two rotations of the normal at the node. The definition of independent rotational and displacement degrees of freedom permits transverse shear deformation to be taken into account, since rotations are not tied to the slope of the mid-surface. The displacements prescribed for in-plane forces do not affect the bending deformations and vice versa.

The displacement components of an arbitrary point within a flat plate element can be expressed as [12]:

$$\begin{pmatrix} u \\ v \\ w \end{pmatrix} = \sum_{i=1}^{n} N_i \left[\begin{pmatrix} u^i \\ v^i \\ w^i \end{pmatrix} + z \begin{bmatrix} \phi_x^i \\ \phi_y^i \\ 0 \end{bmatrix} \right] \tag{3.20}$$

where n is the number of nodes per element, N_i are the known functions of (x,y) known as shape functions, $\{u^i, v^i, w^i, \phi_x{}^i, \phi_y{}^i\}$ are the unknown displacements and rotations at local node i. The above equation (3.20) can be written as,

$$\{u\} = [N]\{u\}^e \tag{3.21}$$

Here, the element displacement vector $\{u\}^e$ is given by :

$$\{u\}^e = \{u^1, v^1, w^1, \phi_x^1, \phi_y^1, u^2, v^2, w^2, \phi_x^2, \phi_y^2, \ldots\ldots\}^T \tag{3.22}$$

and, the shape function matrix is defined by:

$$[N] = \begin{bmatrix} \{N_1\} \\ \{N_2\} \\ \{N_3\} \end{bmatrix} \tag{3.23}$$

where,

$$\{N_1\} = \{N_1 \quad 0 \quad 0 \quad zN_1 \quad 0 \quad N_2 \quad 0 \quad 0 \quad zN_2 \quad 0 \quad . \; . \; . \; .\} \tag{3.24a}$$

$$\{N_2\} = \{0 \quad N_1 \quad 0 \quad 0 \quad zN_1 \quad 0 \quad N_2 \quad 0 \quad 0 \quad zN_2 \quad . \; . \; . \; .\} \tag{3.24b}$$

$$\{N_3\} = \{0 \quad 0 \quad N_1 \quad 0 \quad 0 \quad 0 \quad 0 \quad N_2 \quad 0 \quad 0 \quad . \; . \; . \; .\} \tag{3.24c}$$

Similarly,

$$\delta\{u\} = [N]\delta\{u\}^e \tag{3.25}$$

where, the vector $\delta\{u\}^e$ contains the nodal values of the virtual displacement vector.

3.3.3. Finite element equations

The domain is discretized into n_e number of flat plate element. Then, the strain field is expressed in terms of nodal displacement by using eq. (3.2) and eq. (3.21) as,

$$\{\varepsilon\} = [B]\{u\}^e \tag{3.26}$$

where, $[B]$ is the matrix relating the strain components to the element nodal displacements, and is given by:

$$[B] = [B_1 B_2 \ldots\ldots B_n] \tag{3.27}$$

where,

$$B_i = \begin{bmatrix} \frac{\partial N_i}{\partial x} & 0 & 0 & \frac{\partial (zN_i)}{\partial x} & 0 \\ 0 & \frac{\partial N_i}{\partial y} & 0 & 0 & \frac{\partial (zN_i)}{\partial y} \\ \frac{\partial N_i}{\partial y} & \frac{\partial N_i}{\partial x} & 0 & \frac{\partial (zN_i)}{\partial y} & \frac{\partial (zN_i)}{\partial x} \\ 0 & \frac{\partial N_i}{\partial z} & \frac{\partial N_i}{\partial y} & 0 & \frac{\partial (zN_i)}{\partial z} \\ \frac{\partial N_i}{\partial z} & 0 & \frac{\partial N_i}{\partial x} & \frac{\partial (zN_i)}{\partial z} & 0 \end{bmatrix} \quad i\text{=1 to n} \tag{3.28}$$

Similarly,

$$\delta\{\varepsilon\} = [B]\delta\{u\}^e \tag{3.29}$$

Also, note that,

$$\delta\{\varepsilon_o\} = 0 \tag{3.30}$$

Using expressions (3.25), (3.26), (3.29) and (3.30), eq.(3.18) can be written as,

$$\delta\Pi = \sum_{e=1}^{n_2} (\delta\{u\}^{eT}[K]^e\{u\}^e - \delta\{u\}^{eT}[F]^e) = 0 \tag{3.31}$$

where, $[K]^e$ represents the elemental stiffness matrix defined by,

$$[K]^e = \int_{V^e} [B]^T [D][B] dV \tag{3.32}$$

and, $[F]^e$ represents the elemental force vector given by,

$$[F]^e = \int_{V^e} [B]^T [D] \{\varepsilon_o\} dV + \int_{\Gamma_t^e} [N]^T \left\{ \bar{t} \right\} d\Gamma \tag{3.33}$$

Here, V^e represents the domain of a typical element e and Γ_t^e represents the elemental boundary on which the tractions are specified.

After assembly, the above equation becomes,

$$\delta \Pi = \delta\{u\}^T [K]\{u\} - \delta\{u\}^T [F] = 0 \tag{3.34}$$

where $[K]$ is global stiffness matrix and $[F]$ is global force vector, $\{u\}$ is the global displacement vector and $\delta\{u\}$ is the global virtual displacement vector (or the variation of $\{u\}$). Since $\delta\{u\}$ is arbitrary (except for the degrees of freedom lying on Γ_u), we have

$$[K]\{u\} = [F] \tag{3.35}$$

The evaluation of $[K]^e$ is done using numerical integration. For this purpose, (x, y) coordinates are transformed to the natural coordinates (ξ, η) using the transformation given by eq. (2.30). The z coordinate is transformed to ζ coordinate using the transformation:

$$z = \frac{t\zeta}{2} \tag{3.36}$$

where t is the thickness of the plate. Thus ζ varies varies from -1 on the bottom surface to +1 on the top surface.

In the present work, three nodded flat plate element has been used for the deformation analysis of the mask frame assembly. The elements of the coefficient matrix are numerically integrated using three integration points located at the midpoints of the three sides.

Chapter 4

Test Problems

4.1. Introduction

The shadow mask assembly is analyzed using NASTRAN. To develop the familiarity with NASTRAN, certain test problems are solved. Results of the test problems are presented in this chapter. The following two test problems are solved:

1. 2-D heat transfer problem.
2. Plate bending problem.

4.2. 2-D Heat transfer problem

An isotropic plate subjected to specified temperature on two boundaries and convective heat loss on the remaining boundaries [14] is analyzed using NASTRAN and the results are compared with those from reference [14]. This problem is chosen to validate formulation for the thermal analysis of a flat plate rather than for its practical significance.

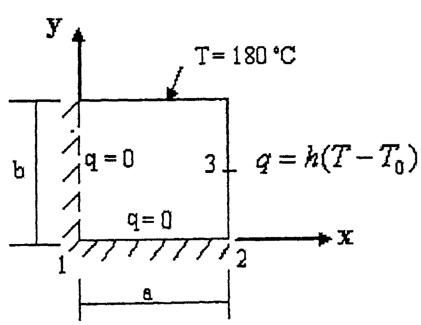

Fig. 4.1 Plate geometry and boundary conditions

Figure (4.1) shows the geometry and boundary conditions of the plate. Only quarter of the plate has been modeled due to the symmetry about the x and y axis. All

specified quantities refer to the quarter plate model. The geometric and material parameters are [14]:

a = 400 mm.

b = 300 mm.

h = 50E-6 W/mm^2 °C.

T = 180 °C.

T_0 = 25 °C.

k = 1.5E-3 W/mm °C.

Three noded triangular element is employed for performing the thermal analysis. The mesh is shown in Fig. 4.2. The discretization details are:

- Number of elements = 2400
- Number of d.o.f. = 3772.

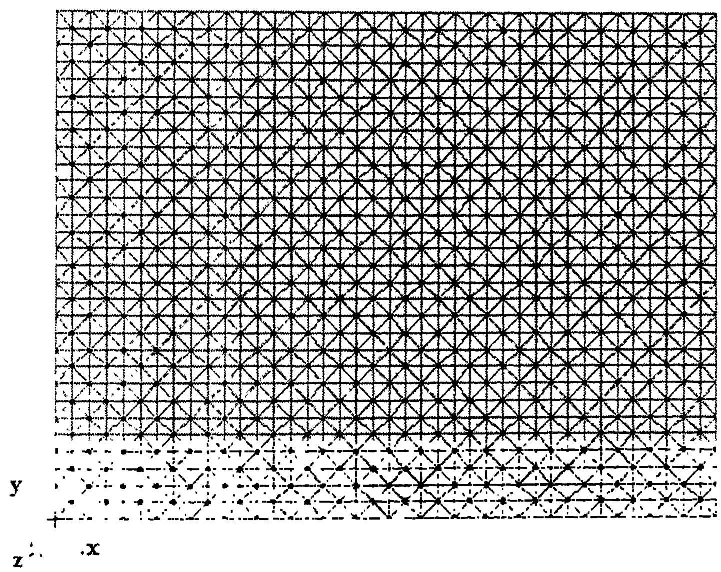

Fig. 4.2 Mesh generated using 3-noded triangular element

The results obtained using NASTRAN together with the results from the reference [14] are presented in a tabular form in Table 4.1. Comparison is carried out at points 1, 2 and 3 shown in Fig. 4.1. From the Table (4.1), it is clear that the temperature at the three points obtained using NASTRAN are in good agreement with

the results from reference [14]. This establishes the validity of the 3 noded triangular element for the thermal analysis of thin plates.

Point No.	Temperature (°C) from reference [14]	Temperature (°C) using NASTRAN
1	124.50	123.9968
2	34.00	39.46054
3	45.40	44.30891

Table 4.1 Comparison of temperature values

4.3. Plate bending problem

A plate fixed at all four edges and subjected to uniform pressure [15] is analyzed using NASTRAN and the results are compared using those from reference [15]. This problem is chosen to validate formulation for the plate bending analysis rather than for its practical significance.

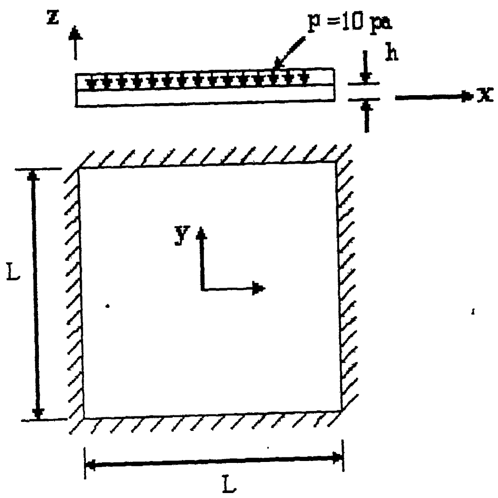

Fig. 4.3 Plate geometry and boundary conditions

Figure 4.3 shows the geometry and boundary conditions of the plate. All specified quantities refer to full plate model. The geometric and material parameters are [15]:

$L = 500$ mm.

$h = 2$ mm.

$E = 200e3$ N/mm^2.

$\upsilon = 0.3.$

$p = 10$ Pa.

The plate is discretized using three noded triangular elements. The mesh is shown in Fig. 4.4. The discretization details are:

- Number of elements = 5000
- Number of d.o.f. = 12005.

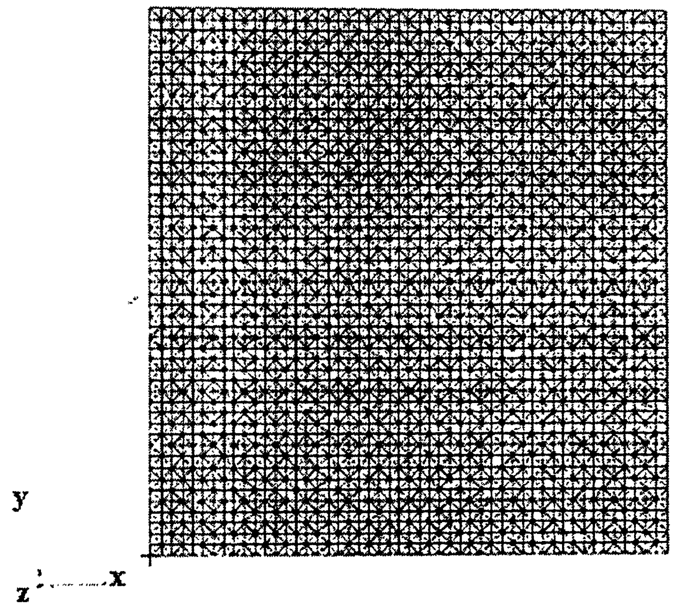

Fig. 4.4 Mesh for plate bending analysis using 3-noded triangle

The results obtained from NASTRAN together with the results from reference [15] are presented in Table 4.2. The maximum displacement obtained from NASTRAN is in good agreement with the results of the reference [15]. This establishes the validity of the use of 3 noded triangular element for bending analysis of thin plates.

Max. displacement(mm) from reference [15]	Max. displacement (mm) from NASTRAN
5.47E-3	5.4E-3

Table 4.2 Comparison of displacement values

Chapter 5

Results and Discussion

The shadow mask assembly is analyzed using NASTRAN based on the formulation presented in chapters 2 and 3. The three noded triangular element has been employed for finite element discretization. Thermo-elastic deformation analysis for the mask frame assembly is performed after analyzing transient temperature distribution in the mask. Finally, the beam landing shift is predicted.

5.1 Problem Statement

The shadow mask consists of a shadow mask with numerous apertures, frame and support springs as shown in Fig. (5.1). The shadow mask and surrounding frame are

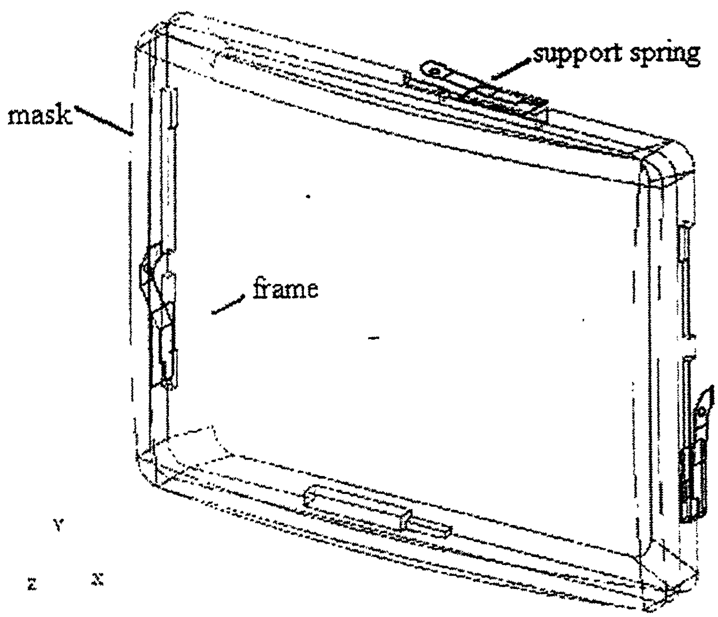

Fig. 5.1 Geometry of the shadow mask

connected by spot welding at several points and the support springs are attached on

the faces of the frame. The shadow mask assembly is supported by the support spring fitted into the tapered stud on the C.R.T. wall. Finite element thermo-elastic analysis is performed to calculate the temperature distribution and corresponding landing shift of electron beams on the panel due to the thermal deformation of the assembly. Since it is impossible to model the mask with numerous apertures, we replace the shadow mask by a thin plate with no apertures. Figure. (5.2) shows the shadow mask modeled as a thin plate. The geometric parameters, boundary conditions and material properties are :

1. **Geometric parameters [3]:**

   Length of mask, A = 404.8 mm.

   Length of portion with apertures, a =387.92 mm.

   Width of mask , B = 306.0 mm.

   Width of portion with apertures, b = 298.12 mm.

   Thickness of mask , h = 0.2 mm.

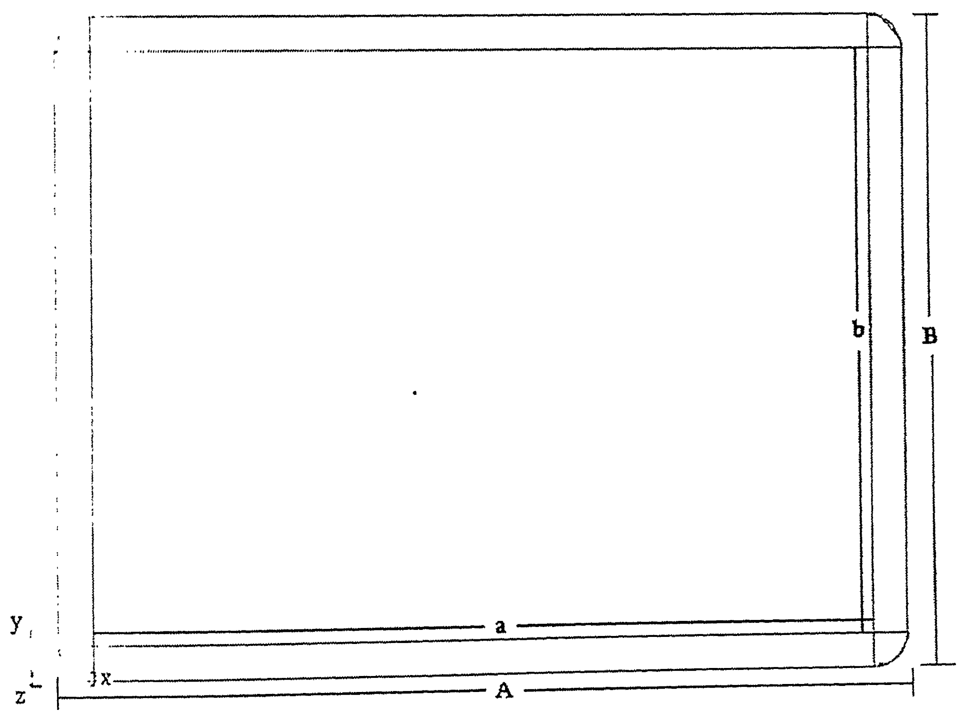

Fig. 5.2 Thin plate model for shadow mask

2. **Boundary Conditions**

   - Input heat flux q_{in} [3]= 210.1 W/mm^2.

- Thermal boundary conditions:

  Insulated at edges.

- Geometric boundary conditions

  Clamped at the edges, u = 0 , v = 0, w=0.

3. Material Properties :

The effective material properties for the mask without apertures and the mask with apertures are shown in Table (5.1) [3] .

Properties	Mask (without apertures)	Mask (with apertures)
Young's modulus (N/mm^2)	2.2E5	1.6E5
Poisson's ratio	0.25	0.26
Specific heat (J/kg °C)	475	475
Conductivity (W/mm °C)	5.45E-2	3.055E-2
Co-eff of thermal expansion (/°C)	1.15E-5	1.15E-5
Emmisivities	0.55	0.87

Table 5.1 Material properties

The geometry of the plate is discretized using the three noded triangular element for both the transient thermal analysis as well as deformation analysis. The discretization details are:

Number of elements = 3584.

Number of d.o.f. = 5613.

5.2 Transient thermal analysis

Transient thermal analysis is performed on the plate model to determine the transient temperature distribution in the shadow mask. Figures (5.3 – 5.7) show the temperature distribution on the shadow mask after 50 seconds, 130 seconds, 250 seconds, 410 seconds and 490 seconds of operation respectively. A steady state is reached approximately at 490 seconds. The maximum temperature occurs at the center of the mask. Figure 5.8 shows the variation of maximum temperature with time

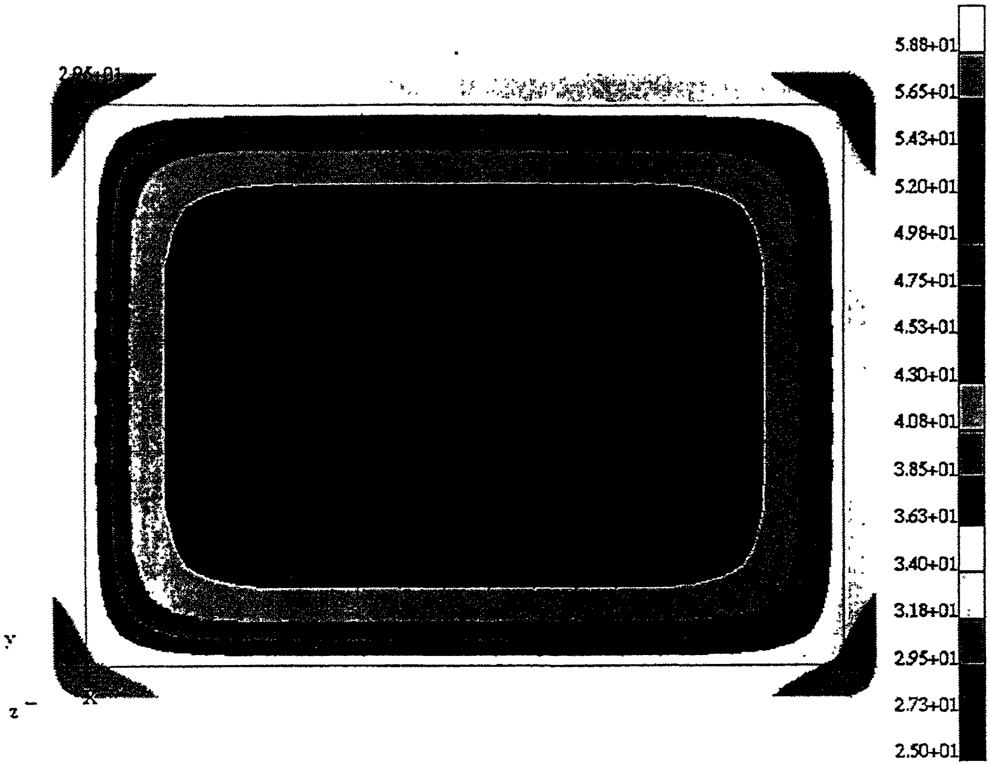

Fig. 5.3 Temperature distribution (at t = 50 sec)

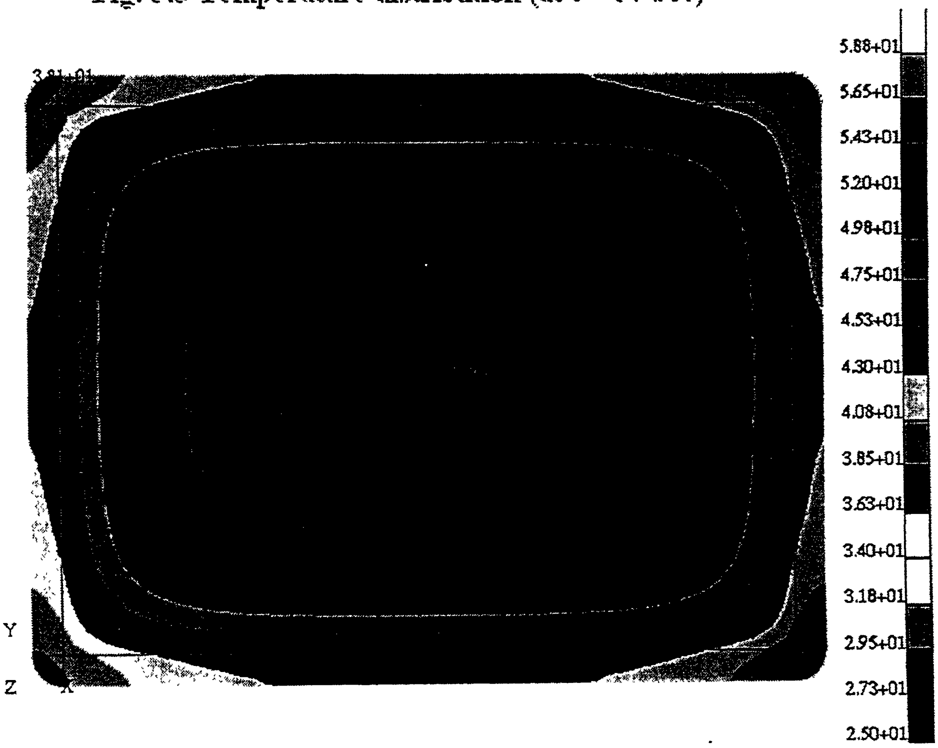

Fig. 5.4 Temperature distribution (at t = 130 sec)

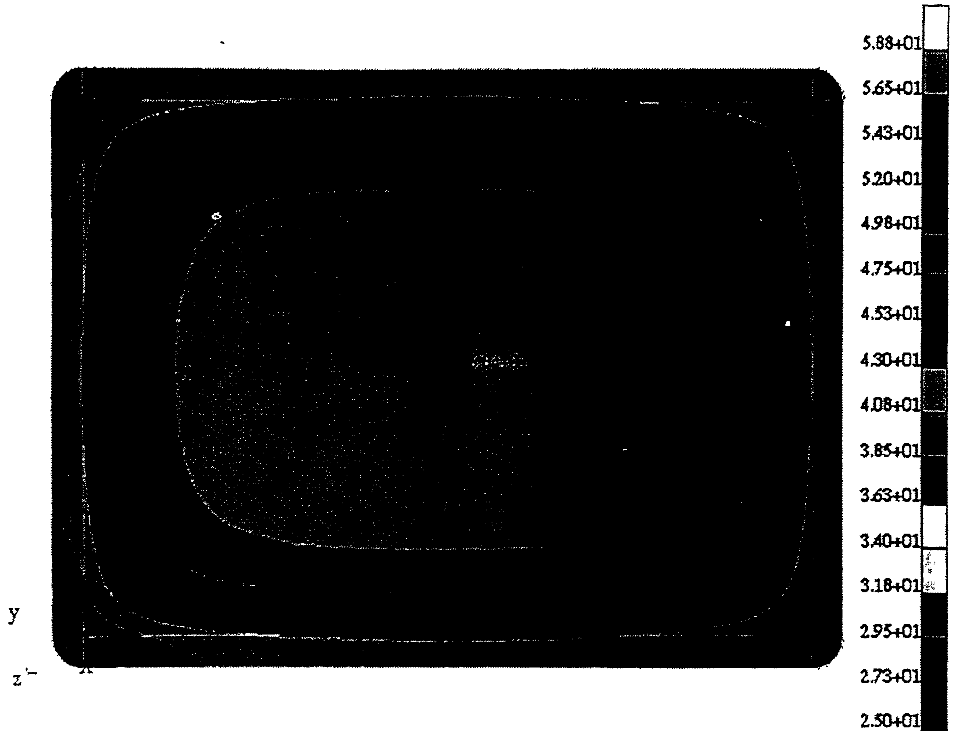

Fig. 5.5 Temperature distribution (at t = 250 sec)

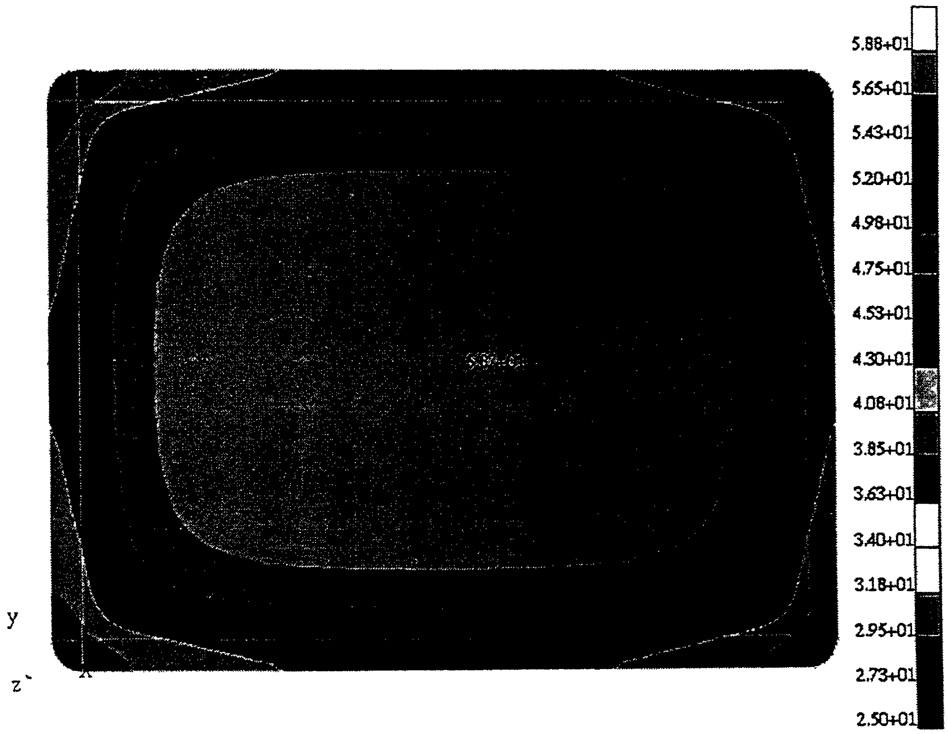

Fig. 5.6 Temperature distribution (at t = 410 sec)

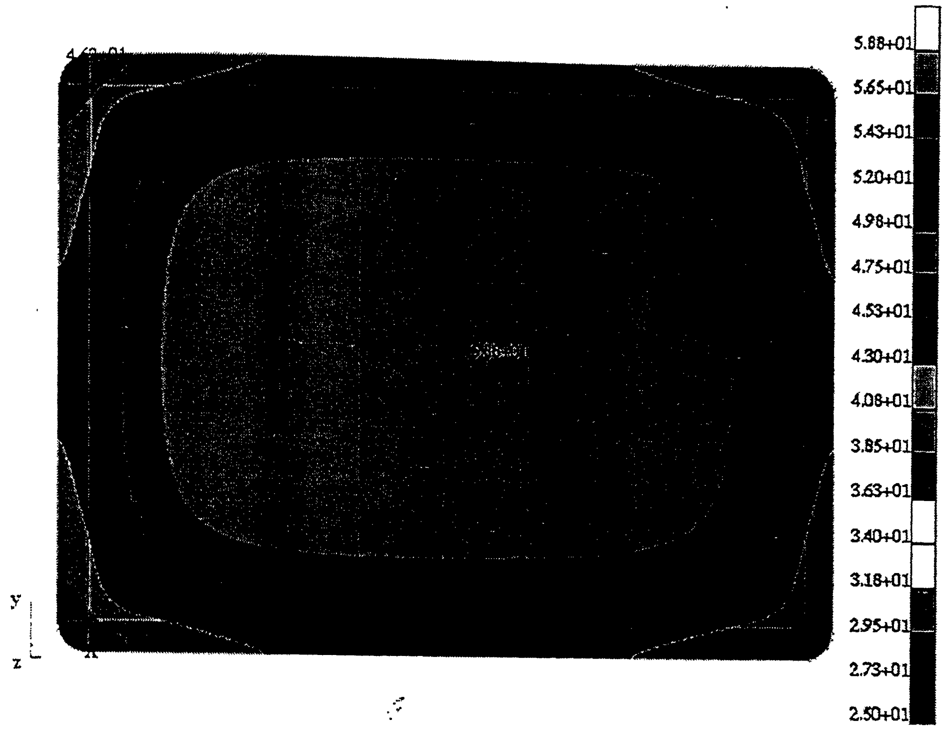

Fig. 5.7 Temperature distribution (at t = 490 sec)

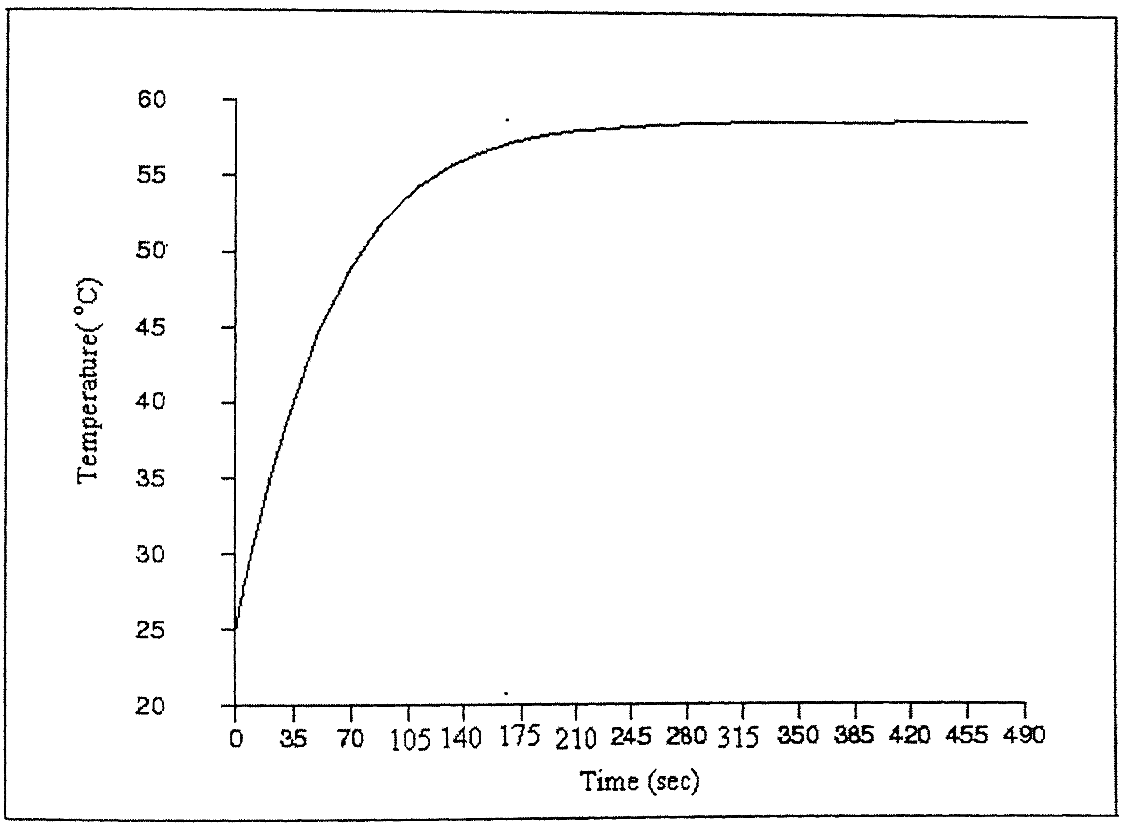

Fig. 5.8 Temperature at center of mask using NASTRAN

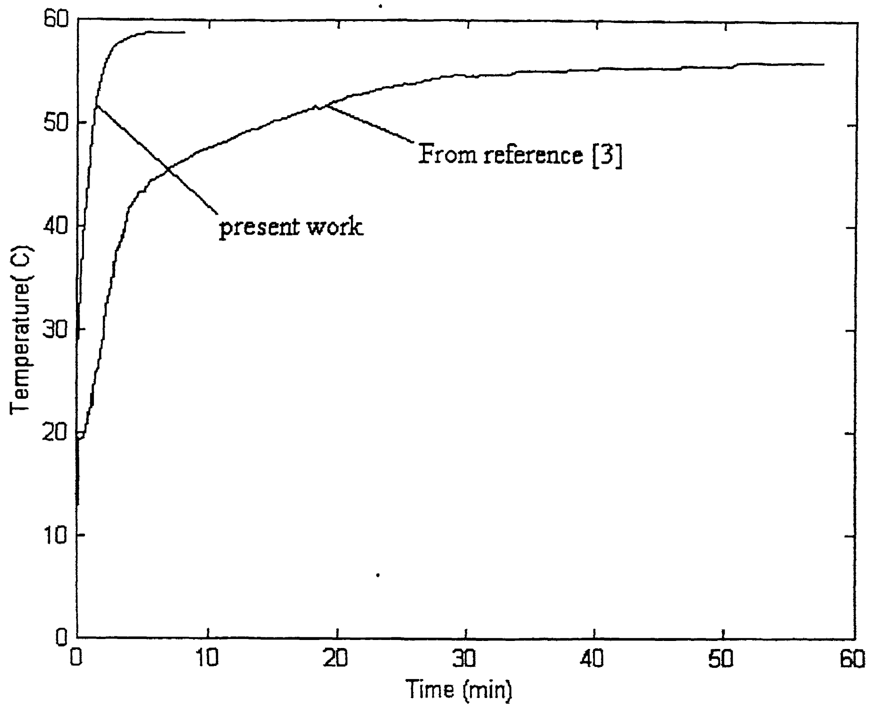

Fig. 5.9 Comparison of temperature distribution with reference [3]

Figure 5.9 compares the results from the present work with the result of reference [3]. From Fig. 5.9 it can be inferred that the trend of temperature distribution for the present work is in agreement with reference [3].

5.2 Thermal deformation analysis

Thermal deformation analysis is performed on the plate model for the shadow mask to estimate the deformation of the mask corresponding to the thermal strain induced in the mask. Figures (5.10 – 5.14) show the contours of beam landing shift on shadow mask after 50 seconds, 130 seconds, 250 seconds, 410 seconds and 490 seconds of operation respectively. Beam landing shift is the magnitude of resultant displacement.

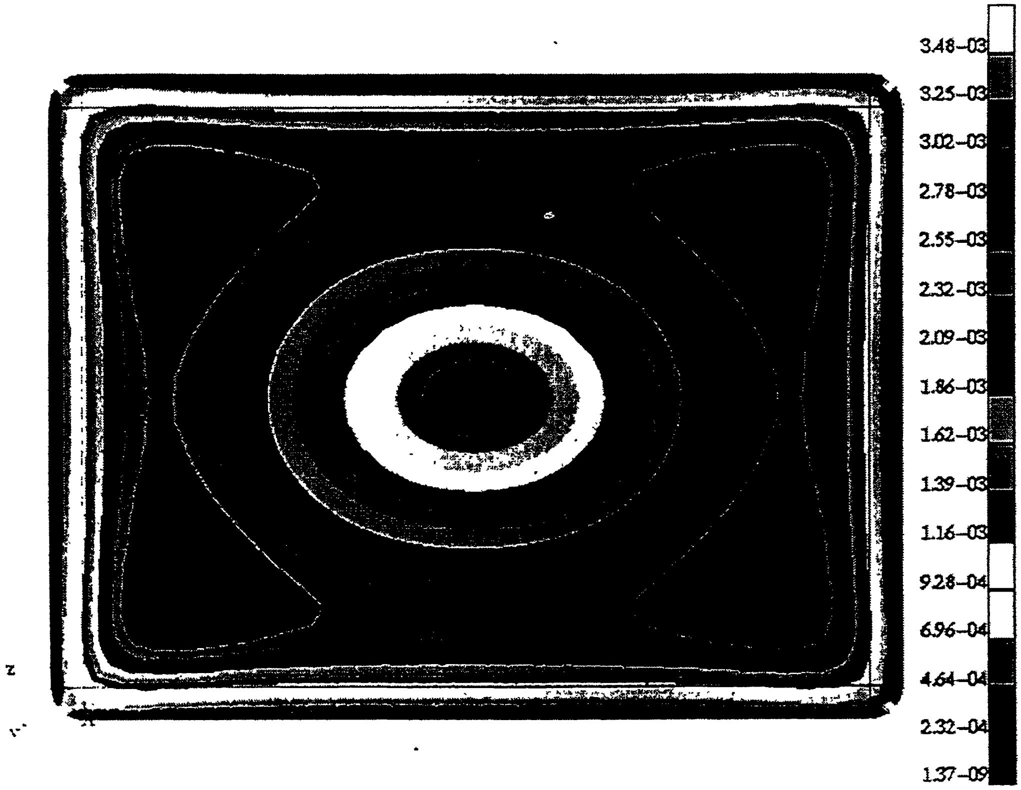

Fig. 5.10 Beam landing shift (at t = 50 sec)

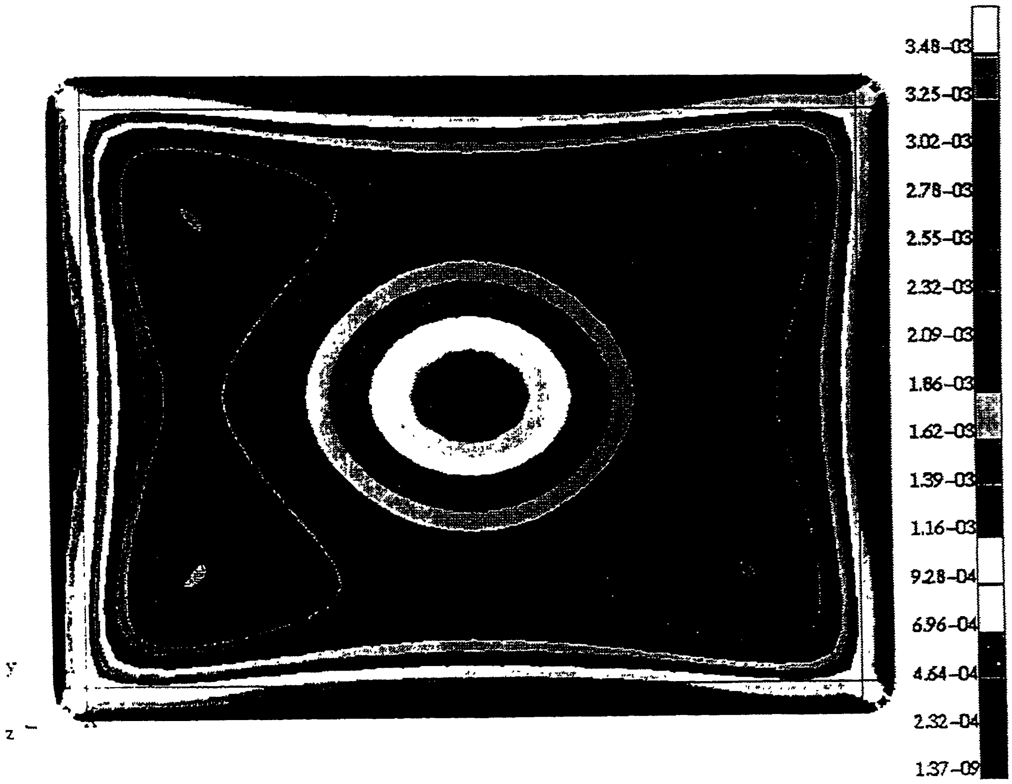

Fig. 5.11 Beam landing shift (at t = 130 sec)

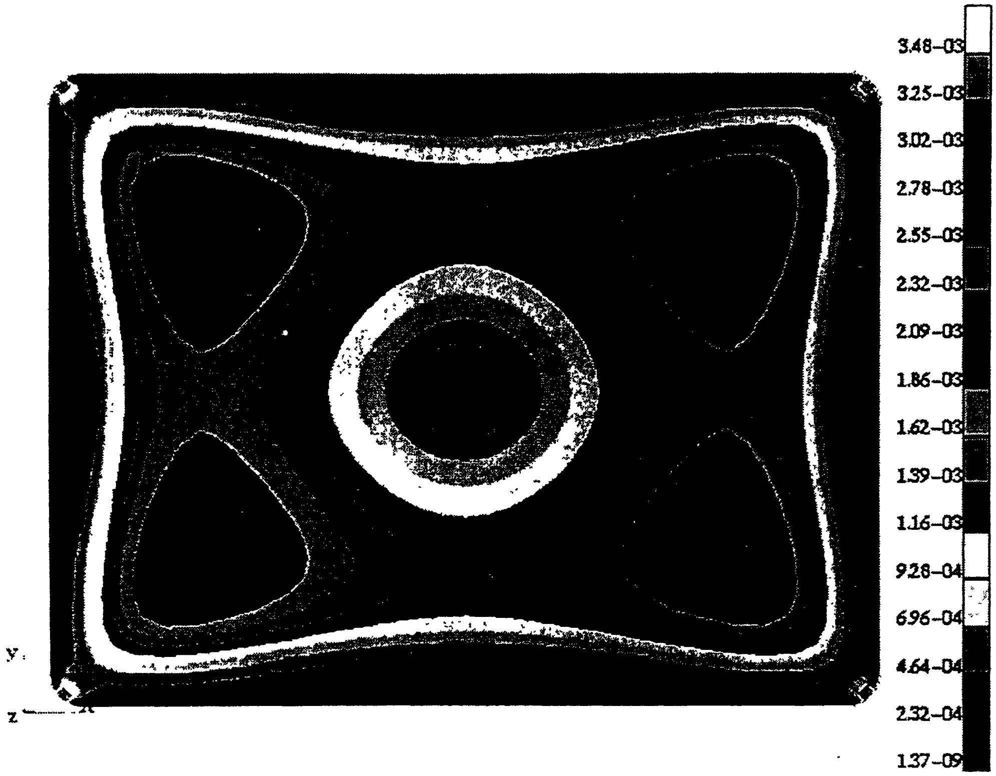

Fig. 5.12 Beam landing shift (at t = 250 sec)

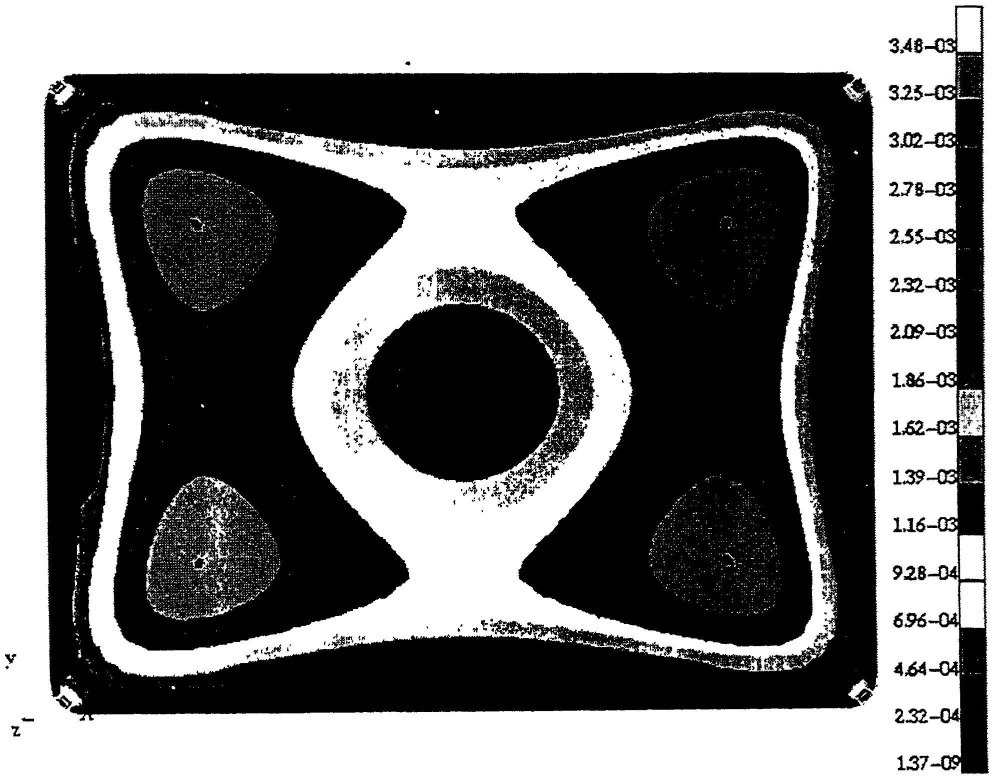

Fig. 5.13 Beam landing shift (at t = 410 sec)

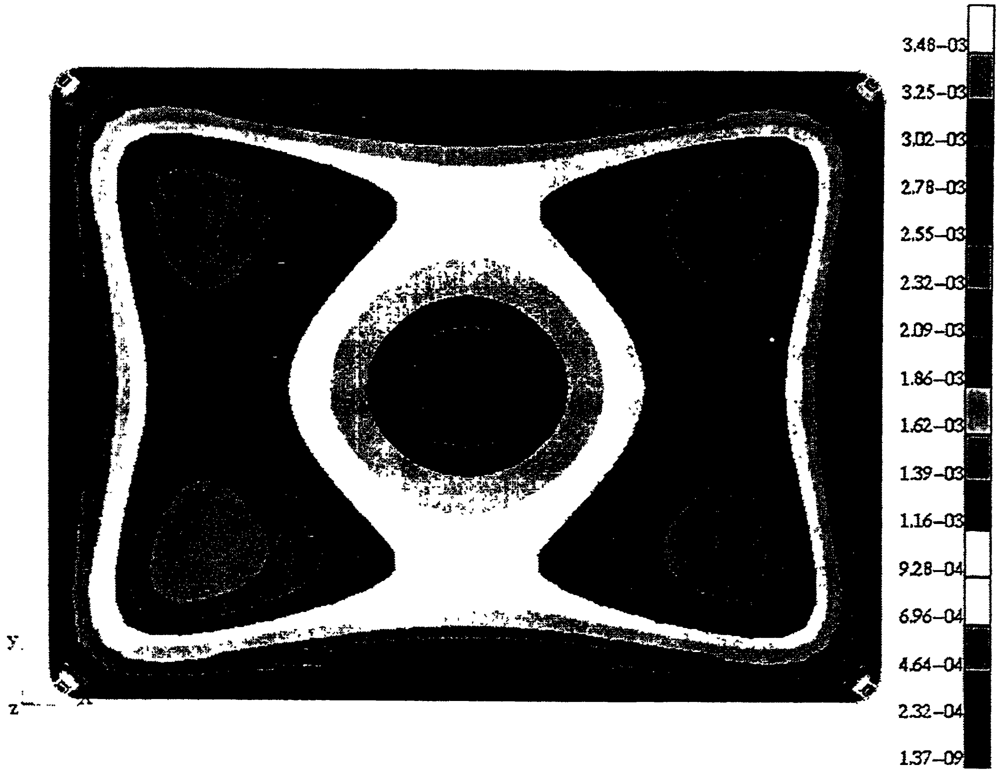

Fig. 5.14 Beam landing shift (at t = 490 sec)

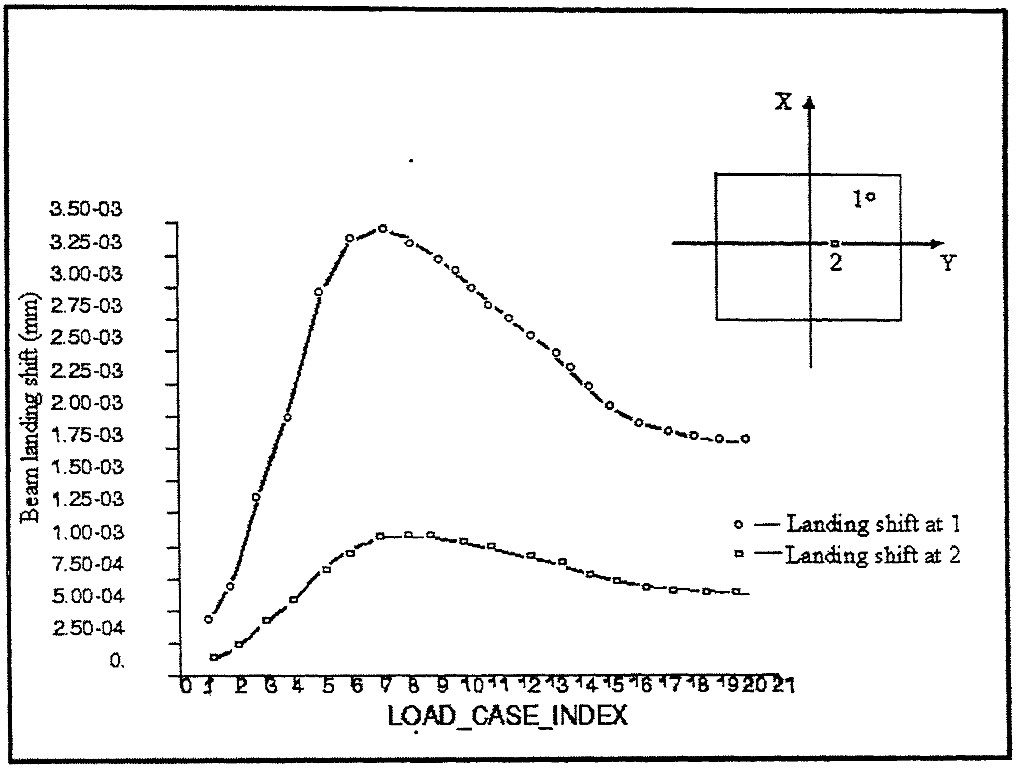

Fig. 5.15 Beam landing shift at positions 1 (188, 133) and 2 (123, 0)

Figure 5.15 shows the variation of beam landing shift with load cases. The load cases correspond to the time steps taken for the transient thermal analysis of the mask. The peak value of beam landing shift (3.48 E-3 mm) occurs at 90 seconds, and thereafter the beam landing shift settles to a lower value as the temperature difference between the center of mask and corner of mask begins to decrease. The present result differs appreciably from that of reference [3]. This discrepancy in the result is due to the difference in the modeling. The shadow mask here has been modeled as a flat plate rather than as a curved surface along with the frame and support springs which will present the actual behavior of the shadow mask response to the thermal deformation.

Chapter 6

Conclusions and Scope for Future Work

6.1 Conclusions

The shadow mask assembly is modeled as a thin plate for predicting beam landing shift due to thermal deformation of the mask. The heat transfer in shadow mask is treated as a 2-D problem and formulation for the thermal analysis of a flat plate is used. The formulation for the plate bending analysis is used to calculate the thermal deformation of the mask under temperature induced strains and displacement boundary conditions. Two test problems are solved to validate the formulation for 2-D thermal analysis and plate bending analysis of flat plate.

The three noded triangular element has been employed for finite element discretization to perform thermo-elastic analysis using NASTRAN. The trend for the temperature distribution in the shadow mask using NASTRAN is in good agreement with the temperature distribution from literature. The trend for the beam landing shift is also in agreement with landing shift from the literature, though the values differ. This discrepancy in the result is due to the difference in the modeling of the shadow mask. This shows that the assumption of modeling the shadow mask as a thin plate can be used to predict the trends of temperature distribution on the mask and the beam landing shift but not their values.

6.2 Scope for Future Work

The present work can be extended in the following directions:

1. The shadow mask can be modeled as a shell and the governing equations for heat transfer and deformation for shell can be used.

2. The whole shadow mask assembly comprising of shadow mask, frame and clips should be analyzed together to precisely predict the landing shift.

References

1. Inaba, M., Teshima, K., Higashinakagawa, E. and Ohtake, Y., (1998), *Development of an Invar (Fe-36Ni) shadow mask for color cathode ray tubes*, IEEE Transactions on Electron Devices, 35, 1721-1729.
2. Kim, K.W., Kang, D.J., Kim and N.W., (1997), *Measurements of the temperature distribution of a shadow mask in a cathode-ray tube by use of a radiation thermometer*, Meas. Sci. Technol., 8, 1328-1332.
3. Kim, H. and Im, S. , (1994) , *Analysis of beam landing shifts due to thermal Deformations of a shadow mask,* IEEE Transactions on Consumer Electronics, 40, 47-54.
4. Tokita, K., Inoue, M., Sone, T. and Urata, H., (1991), *Geometric compensation for mask expansion of colour cathode-ray tubes*, Displays, 74-79.
5. Park, S.K., Kim, J., Chang, Y.C. and Kang, B.S., (2001), *Analysis of the deformation of a perforated sheet under thermal and tension load using finite element method,* Journal of Materials Processing technology, 113, 761-765.
6. Okada, T. and Ikegaki, M., (1983), *A structural analytical study on shadow mask thermal deformation of color CRT*, Japan Display, 20-22.
7. Kim, K.W. and Kim, N.W., (1998), *Analysis of shadow mask thermal deformation and prediction of beam landing shifts for color CRT,* IEEE Transactions on Consumer Electronics, 44, 442-450.
8. Dill, E.H., (1990), *A triangular finite element for thick and thin plates*, Computers & Structures, 35, 301-308.
9. Mortenson, M.E., (1985), *Geometric Modelling*, John Willy & Sons.
10. Jang, B.W., Shin, W.S. and You, S.J., (1998), *Thermal deformation of a tension mask and beam landing shift for a perfectly flat CRT under localized heating, IEEE Transactions on Consumer Electronics*, 45, 243-301.

11. Zienkiewicz, O.C., (1979), *The Finite Element Method,* Tata McGraw-Hill, New Delhi.

12. Hinton, E. and Owen, D.R.J., (1984), *Finite Element Software for Plates and Shells*, Pineridge Press Limited.

13. Sydenstricker, R.M. and Landau, L., (2000), *A study of some triangular discrete Reissner-Mindlin plate and shell elements*, Computers and Structures, 78, 21-33.

14. Chandrupatla, T.R. and Belegundu, A.D., (2001), *Finite Elements in Engineering,* Prentice hall inc.

15. Ventsel, E. and Krauthammer, T., (2001), *Thin Plates and Shells (Theory, Analysis and Applications)*, Marcel Dekker Inc.